Debond crack growth in fatigue along fiber in UD composite with broken fibers

Johannes Eitzenberger and Janis Varna

Dept of Applied Physics and Mechanical Engineering
Lulea University of Technology, Sweden SE 971 87, Lulea, Sweden
Janis.Varna@ltu.se

ABSTRACT

Assuming that Paris law is applicable for individual debond crack propagation along the fiber/matrix interface, the related strain energy release rate in a unidirectional composite is analysed using FEM and also using simple analytical considerations based on self-similar debond crack propagation. Model with axial symmetry consisting of three concentric cylinders is used: partially debonded broken fiber in the middle is surrounded by matrix cylinder which is embedded in a large block of effective composite with properties calculated using rule of mixtures and Halpin-Tsai expressions. It is shown for pure mechanical loading that the fiber elastic properties have a huge effect on the released energy, whereas fiber content in the composite in the considered realistic range has effect only for short debonds. The interaction between debonds approaching from both fiber fragment ends is investigated and related to material properties and geometrical parameters. It is shown that the self-similar debond propagation model gives slightly overestimated values of the strain energy release rate which may be related to interaction effects not included in the analytical model.

1. INTRODUCTION

Since the fiber strain to failure in polymer matrix fiber reinforced unidirectional (UD) composites is lower than the matrix strain to failure the first failure event in tensile loading in these composites is statistical fiber failures. Due to stress transfer over the interface the stress in the fiber is recovered and with increasing load multiple fiber breaks in are possible.

Very often the fiber failure, which is assumed to be a penny-shaped crack transverse to the fiber axis, is an unstable phenomenon and the energy released during this event is larger than required. The excess of energy may go to initiation of the fiber/matrix debond at the tip of the fiber crack. In other words the debonding is a creation of free fiber surface growing along the fiber in the axial direction. The debond initiation (transition from “no debond” state to “debond” state) is very complex process and due to lack of relevant information it is not suitable for fracture mechanics treatment.

The debonding can be considered as an interface crack growth along the fiber and fracture mechanics may be used for the crack evolution analysis. The stress state at the fiber crack and in the debond tip region is very complex. For long debonds plateau region exists away from the fiber crack and from the debond crack tip. Due to further debond crack growth the plateau region becomes larger. Long debond cracks propagate in a self-similar manner meaning that when the crack grows the local stress profile at the debond crack front shifts along the fiber axis without changes in the shape and in the value. Very long debonds (comparable with the half-length of the fiber fragment) start to interact and the self-similarity is lost.

The energy release rate during debond propagation has been previously calculated for debond along a single fiber fragment embedded in an infinite matrix in so called single fiber fragmentation (SFF) test. The used methods cover a wide spectrum from approximate

analytical to numerical based on finite elements (FE) or boundary elements (BE) [1-7]. The variational model based on minimization of the complementary energy [1] is probably one of the best analytical solutions but the accuracy is achieved in rather complex calculation routine. The most careful numerical analysis of the local stress state at the debond crack tip in terms of stress intensity factors and degree of singularity has been performed in [6] using BE method. Unfortunately this method at present is limited to isotropic constituents and, hence, not applicable for carbon fibers. Generally speaking, most of the described approaches may be adapted for dealing with partially debonded broken fiber surrounded by matrix in a composite. However a systematic parametric analysis of the energy release rate as affected by constituent properties, geometrical parameters is not available.
The objective of this paper is to perform the abovementioned analysis using FE and to identify the most significant parameters influencing the strain energy release rate. A three concentric cylinder assembly model is considered. A broken fiber in the middle is surrounded by a matrix cylinder and the interface is partially debonded, see Fig.1. This fiber /resin block is embedded in outer "effective composite" cylinder.

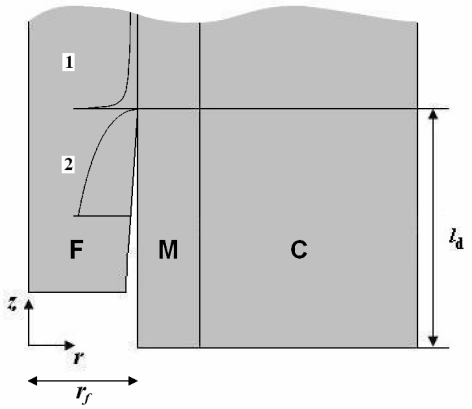

Figure 1: Schematic showing the three cylinder geometry with the partially debonded fiber in the middle. The stress distribution in the front of the debond crack and the displacement profile behind the crack are indicated.

2. MODE II ENERGY RELEASE RATE G_{II}

In the particular case of the debond crack the radial stresses on the fiber surface are compressive. It is due to larger Poisson's ratio of the matrix and also due to higher thermal expansion coefficient (if thermal stresses are accounted for). This means that the crack propagation in the analysed problem is in Mode II. Effects related to friction at the interface are neglected.
In fatigue Paris law may be applied which requires the change of the strain energy release rate to be calculated.

$$dl_d / dN = A\left(\frac{\Delta G_{II}}{G_{IIc}}\right)^{\beta} \qquad (1)$$

The unit cell of the composite with a partially debonded fiber is shown in Fig.1. The radius of the transversally isotropic fiber is r_f. The outer radius of the matrix cylinder r_m is related to the fiber content in the composite by $V_f = \left(r_f / r_m\right)^2$. To represent the infinite effective composite surrounding the fiber/matrix unit, the outer radius of the cylinder assembly R is large.

2.1 The crack closure technique

The energy release rate is calculated using the virtual crack closure technique [8] stating that the energy released due to the crack surface growth by dA is equal to the work required to close this newly created surface from size $A + dA$ back to size A. For the debond crack

$$dA = 2\pi r_f dl_d \tag{2}$$

Points at the debonded surfaces of a crack with size $l_d + dl_d$ are sliding with respect to each other the relative displacement being

$$u^{l_d+dl_d}(z) = u_{fz}^{l_d+dl_d}(z, r = r_f) - u_{mz}^{l_d+dl_d}(z, r = r_f) \qquad z \in [0, l_d + dl_d] \tag{3}$$

To close the crack by dl_d we have to apply an increasing tangential traction at each point $z \in [l_d, l_d + dl_d]$ to move it back by $u^{l_d+dl_d}(z)$. When it is done the value of the traction in point z equals to $\sigma_{zr}^{l_d}(z)dz$, where $\sigma_{zr}^{l_d}(z)$ is the shear stress in front of a crack with size l_d. The work performed equals to

$$dW = \frac{1}{2} u^{l_d+dl_d}(z)\sigma_{zr}^{l_d}(z)dz \tag{4}$$

In the virtual crack closure technique the assumption is that the sliding displacement field at the tip of the crack with size $l_d + dl_d$ is the same as at the tip of the debond with size l_d

$$u^{l_d+dl_d}(z) = u^{l_d}(z - dl_d) \tag{5}$$

This assumption is based on the assumed self-similarity of the crack growth between l_d and $l_d + dl_d$ which is a good assumption as long as dl_d is "small". The benefit of this assumption is that only one stress state calculation for a given debond length l_d is required. From (4) and (5) follows expression for the work performed to close the crack by dl_d

$$W = 2\pi r_f \frac{1}{2} \int_{l_d}^{l_d+dl_d} u^{l_d}(z - dl_d)\sigma_{zr}^{l_d}(z)dz \tag{6}$$

Changing the origin to l_d by introducing $z' = z - l_d$, equation (6) turns to

$$W = 2\pi r_f \frac{1}{2} \int_0^{dl_d} u^{l_d}(z' + l_d - dl_d)\sigma_{zr}^{l_d}(z' + l_d)dz \tag{7}$$

The energy release rate (G) is defined as $G_{II} = \frac{W}{2\pi r_f dl_d}$ which using (7) gives

$$G_{II}(l_d) = \lim_{dl_d \to 0} \frac{1}{2dl_d} \int_0^{dl_d} u^{l_d}(z' + l_d - dl_d)\sigma_{zr}^{l_d}(z' + l_d)dz \tag{8}$$

In numerical calculations dl_d is usually finite and the calculated energy release rate value depends on the integration distance dl_d. The calculated value is called "energy release rate over distance dl_d". This quantity denoted $G_{II}^{dl_d}$ is analysed in the present paper.

2.2 Self-similar debond crack growth region

If the debond length is several times larger than the fiber radius, the stress state at the fiber crack is not interacting with the stress state at the debond crack tip. Additionally assuming that the fiber fragment is long enough and the interaction with the debond approaching from the other end of the fiber is negligible one may state that the debond is growing in a self similar manner. It means that due to debond growth by dl_d the stress perturbation region at the debond tip is shifted in the z-direction by dl_d without any changes in the stress profiles and values. From other hand the complex stress state region at the fiber crack tip remains unchanged. Thinking in terms of the change of the strain energy of the whole system we can observe that the energy change analysis is very straightforward: a region with the volume $\pi R^2 dl_d$ which previously had the strain energy as for long three cylinder assembly with perfectly bonded interfaces is now replaced by the same volume where the fiber cylinder is separated (debonded) from the rest of cylinders. Denoting the strain energies for these two states by indexes 0 and 1 and for simplicity *neglecting thermal terms* we obtain

$$\Delta U = U_1 - U_0 = \frac{\pi R^2 dl_d}{2} \varepsilon_0^2 \left(E_1 - E_0\right) \tag{9}$$

In (9) E_0 and E_1 is the elastic longitudinal modulus of the considered part of the cylinder assembly in the initial state (perfect bonding) and in the final state (debonded fiber). The elastic modulus change between two cases may be calculated using FEM but there is also an exact analytical solution available [9,10,11]. This solution is used to calculate the elastic moduli. Additional assumption made is that in the debonded case the radial stresses due to the presence of the debonded fiber inside the assembly may be neglected and the strain energy of the debonded fiber in the zero friction case is equal to zero. The strain energy release rate is calculated as

$$G_{II} = -\left.\frac{\Delta U}{2\pi r_f dl_d}\right|_{\varepsilon=\varepsilon_0} \tag{10}$$

leading to

$$G_{II} = \frac{R^2}{4r_f} \varepsilon_0^2 \left(E_0 - E_1\right) \tag{11}$$

As an alternative to the concentric cylinder assembly model the rule of mixtures can be used to calculate elastic moduli in (11).

3. RESULTS AND DISCUSSION

Calculations were performed for carbon fiber and for glass fibers in polymeric matrix. The used elastic properties of the matrix are

$$E_m = 3 \text{ GPa} \qquad \nu_m = 0.4 \tag{12}$$

The isotropic glass fiber has properties

$$E_f = 70 \text{ GPa}, \qquad \nu_f = 0.2 \tag{13}$$

The elastic properties of the transversally isotropic carbon fiber are as follows

$$E_{fL} = 500\,\text{GPa}, \quad E_{fT} = 30\,\text{GPa}, \quad G_{fLT} = 20\,\text{GPa}, \quad \nu_{fLT} = 0.2, \quad \nu_{fT3} = 0.45 \tag{14}$$

The properties of the effective composite were calculated using the rule of mixtures for longitudinal modulus and Poisson's ratio and Halpin-Tsai relationships for transverse modulus and shear modulus.

The fiber radius used in calculations was $r_f = 4\mu m$. The thickness of the matrix cylinder was calculated from the fiber volume fraction in the composite using (1) and is varying with V_f. The thickness of the effective composite cylinder was $5r_f = 20\mu m$.

FEM calculations were performed on one half of the fiber fragment using the commercial code ANSYS in an axi-symmetric formulation. The PLANE82 plane element, which is a 2-D, second order element with relatively high accuracy was used in a non-uniform mesh consisting of both triangular and rectangular elements. To obtain higher accuracy a refined mesh (of triangular elements) was used in the vicinity of the crack tip and at the end of the debond zone.

Symmetry condition was applied on $z = 0$, $r \in [r_f, R]$, where R is the outer radius of the fiber-matrix-composite system. The axial symmetry is with respect to the z-axis. Displacement in nodes on the side $r = R$, $z \in [0, L_f]$, are coupled in the r-direction. ($L_f = 90r_f$ is the nominal length of the system in the axial direction representing one half of the distance between two fiber cracks which is $2L_f$.) Constant displacement is applied in the z-direction at $z = L_f$, $r \in [0, R]$. The applied axial strain to the assembly was $\varepsilon_0 = 1\%$.

The sliding displacement is shown in Fig. 2. Axial coordinate $z = 20\mu m$ corresponds to the debond tip. It can be seen that the axial displacement of the fiber is almost the same along the whole fiber surface in the studied coordinate interval, whereas, the displacement of the surface of the matrix at the tip of the debonded zone is twice as large as the displacement at $r_f/2$ from the tip of the debond zone. Accordingly, the strong coordinate dependence of the relative motion of the fiber and the matrix ($u_{,fz} - u_{,mz}$) at the fiber/matrix interface with the axial coordinate is due to the displacement of the surface of matrix.

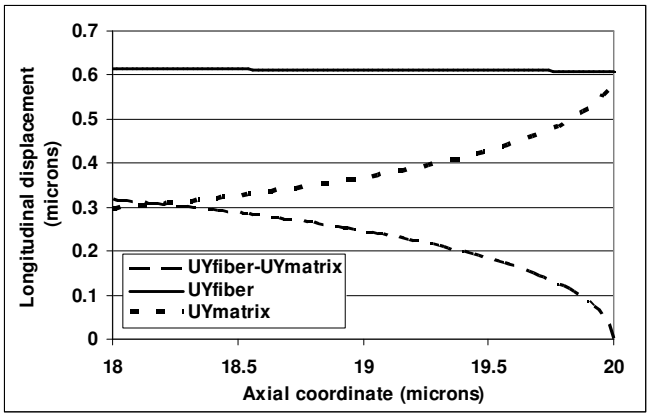

Figure 2: Sliding displacements at both debond faces and the relative sliding given by (3). Carbon/epoxy composite with $V_f = 0.55$, $2L_f = 180r_f$, $l_d = 5r_f$, friction coefficient $k = 0$.

The energy release rate G_{II} was calculated according to (8) and its dependence on the length of the integration region dl_d. It was found that for small values of the ratio dl_d / r_f the calculated values decrease due to insufficient accuracy of the used mesh in the local singular stress state region. For large values the calculated values do not have the meaning of strain energy release rate defined for small crack increments. As a compromise the value corresponding to $dl_d / r_f = 0.1$ has been used to calculate G_{II} throughout this paper.

In Fig. 3 the energy release rate G_{II} when composite volume fraction V_f = 0.45 is compared with V_f = 0.55 for carbon/epoxy and glass/epoxy. It can be seen that for medium to large debond lengths G_{II} is about the same independently of V_f. For short debond lengths, close to the fiber radius, the strain energy release rate in both materials is larger and the values of G_{II} for higher fiber content are lower.

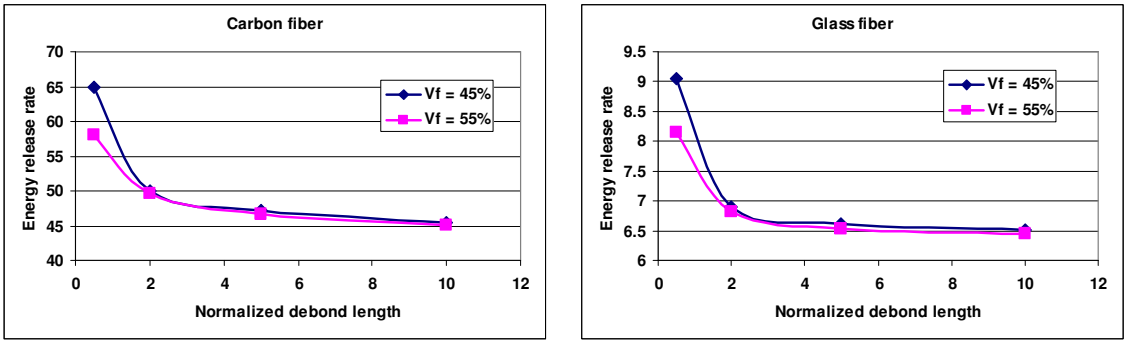

(a) (b)

Figure 3: Strain energy release rate G_{II} versus normalized debond length l_d / r_f in composites with V_f = 0.45 and 0.55 for carbon/epoxy (a) and glass/epoxy (b).

The fiber in this calculation was sufficiently long ($L_f = 90 r_f$) insuring that the debond crack does not interacting with the symmetrical crack on the other end of the fragment.

In Fig. 4 and Fig. 5 the effect of the fiber fragment length on the calculated values of the strain energy release rate G_{II} is presented. The G_{II} dependence on normalized debond length l_d / r_f is shown for different fiber lengths for carbon/epoxy respective glass/epoxy. It can be seen in Fig. 5 that in carbon fiber composite the G_{II} decreases with increasing debond length. This rather linear trend is observed for all fiber lengths and the shorter the fiber is the stronger is the dependence. This is because the same debond length constitutes a larger part of a shorter fiber than of a longer fiber. For short fiber fragments the intact part of the fiber is much smaller and the interaction with the debond approaching from the other fragment end is larger. According to Fig. 4 there is no plateau region in the strain energy release rate which means that the interaction in carbon fiber case starts with very short debond length even for the longest fiber fragment.

It can be seen in Fig. 5 that the overall trend is the same for debond growth in glass/epoxy. The G_{II} decreases with increasing debond length for all fiber lengths. The shorter the fiber is the larger is the dependence on the debond length. This means that the decrease is smaller for glass/epoxy than for carbon/epoxy. In other words, the interaction between debonds from both fiber fragment ends is smaller in glass fiber composite case.

To gain a deeper insight in the nature of the interaction leading to the demonstrated overall trend of G_{II} decrease with increasing debond length the data from Fig. 4 and Fig. 5 are presented as function of fiber length for fixed length of the debond, see Fig. 6 and Fig. 7.

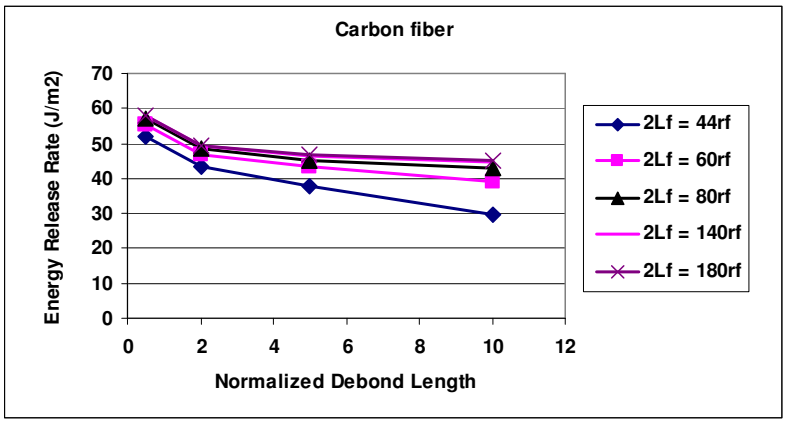

Figure 4: The interaction effect on strain energy release rate G_{II} in carbon/epoxy composite versus normalized debond length l_d / r_f for different fiber lengths, Vf = 0.55.

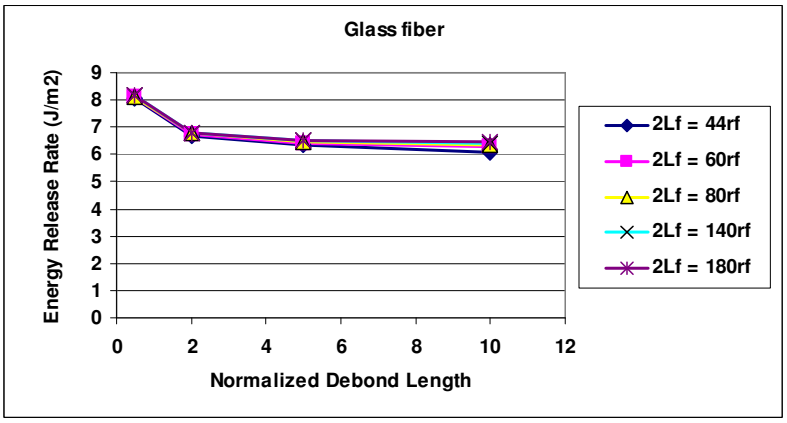

Figure 5: The interaction effect on strain energy release rate G_{II} in glass/epoxy composite versus normalized debond length l_d / r_f for different fiber lengths, Vf = 0.55.

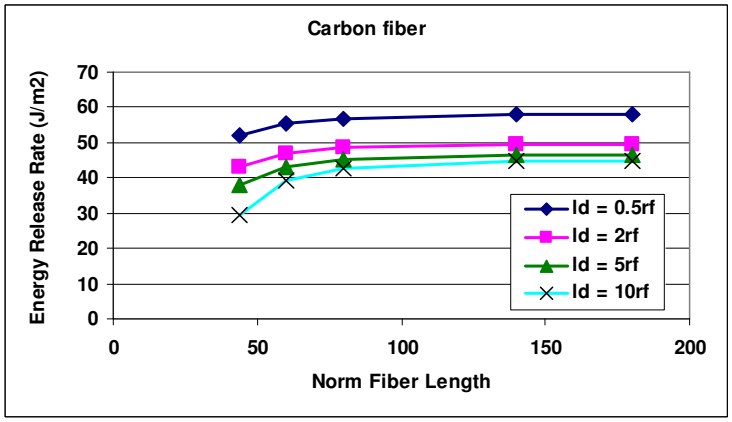

Figure 6: Strain energy release rate G_{II} for debond growth in carbon/epoxy composite versus normalized fiber length $2L_f / r_f$ for different debond lengths when $V_f = 0.55$.

It can be seen in Fig. 6 for carbon/epoxy that the G_{II} decreases with decreasing fiber length for all debond lengths. The larger the debond length is the larger is the dependence on the

fiber length. The reasons for that are explained above. The decrease in G_{II} going from fiber length $180r_f$ to $44r_f$ is between 10 and 34% depending on the debond length.
The strain energy release rate in glass/epoxy composite, which can be seen in Fig. 7, follows the same trends as in carbon/epoxy. However, the dependence on the fiber length in glass/epoxy is not as strong as in carbon/epoxy. The decreases in G_{II} going from fiber length $180r_f$ to $44r_f$ is between 1 and 5%.

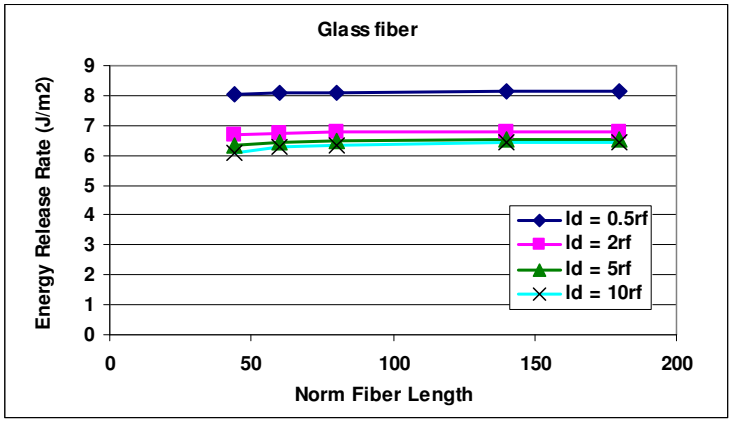

Figure 7: Strain energy release rate G_{II} for debond growth in glass/epoxy composite versus normalized fiber length $2L_f / r_f$ for different debond lengths when Vf = 0.55.

The fact that G_{II} for debond growth in glass/epoxy composite has a weaker dependence on the fiber length compared to carbon/epoxy is related to the differences in the stress distribution (plateau value) in both fibers as shown in Fig. 8 and Fig. 9. It can be seen that the decrease of the plateau value and the length of this zone with decreasing fiber length is much smaller for glass/epoxy (Fig. 9) than for carbon/epoxy (Fig. 8). The difference can be explained by the difference in elastic modulus. The higher the ratio E_{fz} /E_m, the longer is the distance needed to reach the plateau value in the axial fiber stress. For carbon/epoxy the ratio is 500/3 and for glass/epoxy the ratio is 70/3. Thus, due to lower modulus the stress recovery is faster in glass fiber case which leads to smaller stress perturbation zone which in turn results in the weaker dependence for G_{II} on the fiber length.

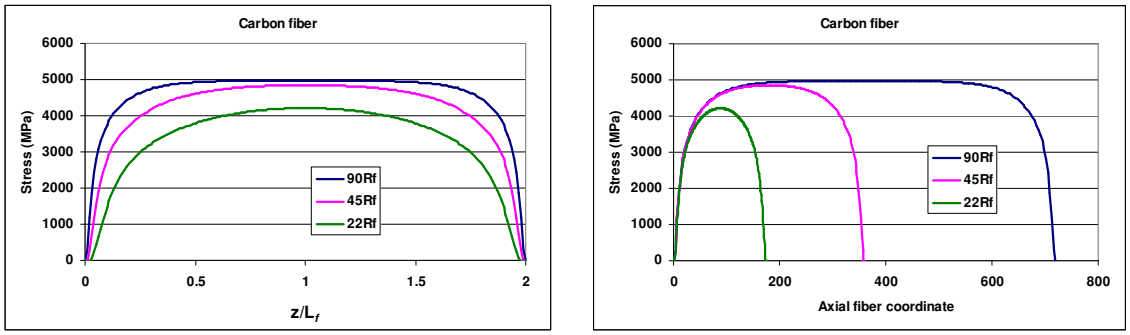

(a) (b)

Figure 8: Axial fiber stress distribution when V_f = 55% and l_d = 0 in carbon fiber versus normalized axial coordinate z / L_f (a) versus axial coordinate (b).

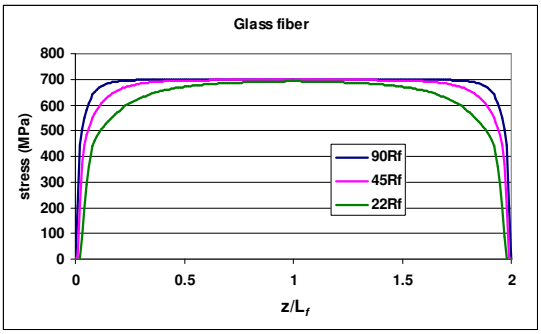

(a)

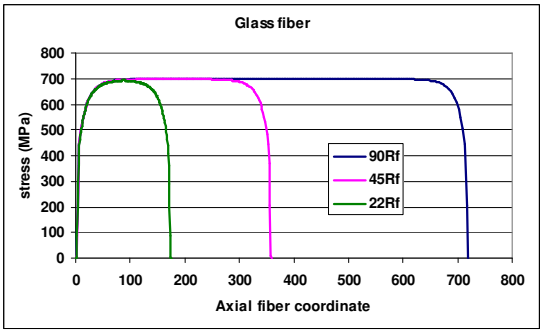

(b)

Figure 9: Axial fiber stress distribution when V_f = 55% and l_d = 0 in glass fiber versus normalized axial coordinate z/L_f (a) versus axial coordinate (b).

Using the expression (11) for strain energy release rate which is valid in the region of self – similar debond crack growth we obtain the following G_{II} values

1. Using concentric cylinder assembly model [11]

For carbon fiber composite

$V_f = 0.45 \quad G_{II}$ =50 J/m^2

$V_f = 0.55 \quad G_{II}$ =50 J/m^2

For glass fiber composite

$V_f = 0.45 \quad G_{II}$ =7 J/m^2

$V_f = 0.55 \quad G_{II}$ =7 J/m^2 (15)

2. Using Rule of mixtures

The results with the used accuracy coincide with results from cylinder assembly model.

The obtained values for the self-similar debond cracks do not depend on the fiber content in the composite. For long debonds this result was also obtained from FEM. The numerical values are slightly higher than obtained by FEM. One explanation for this is that according to FEM there always was an interaction between cracks lowering the G_{II} values. This interaction is not accounted for in the self-similar crack model. Another reason for differences may be that in the concentric cylinder model we have neglected the compressive radial pressure from the debonded fiber to the matrix/effective composite system. It has to be noted that the calculated values of G_{II} are proportional to the fiber modulus, see (13) and (14).

Certainly, the presented results for mechanical loading case have to be superimposed with results for thermal stresses.

4. CONCLUSIONS

The strain energy release rate in Mode II related to fiber/matrix interface debond growth along the fiber surface in unidirectional composites is analysed using FEM considering mechanical stresses only. The parametric analysis performed to reveal the significance of constituent properties, fiber volume fraction fiber fragment length and the debond length on the G_{II} lead to following conclusions.

- The G_{II} is proportional to the fiber modulus and is much larger in carbon fiber composite
- The fiber volume fraction has no effect on the G_{II} for long debonds whereas for short debonds it is larger for lower volume fraction V_f

- The interaction between debonds from both fiber fragment ends decreases the G_{II} values this effect being stronger in carbon fiber composites. The difference is caused by higher stress recovery rate in glass fiber composites due to lower elastic modulus.
- The self-similar debond propagation model with strain energy changes calculated using concentric cylinder assembly solution give a good approximation of the G_{II}. The numerical values are by 5-10% higher than obtained using FEM.

The obtained results will be used to simulate debond growth during fatigue loading.

5. REFERENCES

1. Wu, W., Verpoest, I. & Varna, J., *A novel axisymmetric variational analysis of the stress transfer into fibre through a partially debonded interface*, Composites Science and Technology, 58, (1998) 1863-1877.
2. Nairn J.A. and Liu Y.C., *Stress transfer into a fragmented, anisotropic fiber through an imperfect interface*. Int. J Solids Structures, 1997; 34: 1255
3. McCartney L.N., *New theoretical model of stress transfer between fibre and matrix in auniaxially fibre- reinforced composite.* Proc. R. Soc. London A, 1989; 425: 215-244.
4. R. Joffe, J. Varna and L.A. Berglund, *Analysis of Single Fiber Fragmentation Data,* 3rd Int. Conf. on Deformation and Fracture of Composites, 27-29 March, 1995, Guildford, UK, pp.126-131.
5. J.Varna, R. Joffe and L.A. Berglund, *Interfacial toughness evaluation from the single-fibre fragmentation test,* Composite Science and Technology, vol.56, 9 (1996), 1105-1111.
6. Graciani E, Mantič V, París F and Varna J. *Single fiber fragmentation test. A BEM analysis*. Collection of Technical Papers - AIAA/ASME/ASCE/AHS/ASC Structures, Structural Dynamics and Materials Conference, 2:988-997, Norfolk (Virginia), United States, 2003.
7. W.Wu, I.Verpoest and J. Varna, *Prediction of energy release rate due to the growth of interface crack by variational analysis*, Composites Sci and Technology, 60, (2000), 351-360.
8. Irwin G.R., Fracture, Handbuch der Physik, vol.5, Berlin: Springer Verlag, 1958. p.551.
9. Hashin Z, Rosen BW., 1964, *"The elastic moduli of fiber-reinforced materials",* Journal of Applied Mechanics, 31(2), 223-232.
10. Hashin Z., 1983, "*Analysis of Composite Materials – a Survey*", Journal of Applied Mechanics, 50, 481-505.
11. E. Marklund, J. Varna, R. C. Neagu, E. K. Gamstedt, *"Stiffness of aligned wood fiber composites: Effect of microstructure and phase properties",* Journal of Composite Materials, 2008, accepted.